

# Spherical-Oblate Shape Coexistence in $^{94}\text{Zr}$ from a Model-Independent Analysis

N. Marchini,<sup>1,2,\*</sup> M. Rocchini,<sup>1</sup> M. Zielińska,<sup>3</sup> A. Nannini,<sup>1</sup> D.T. Doherty,<sup>4</sup> N. Gavrielov,<sup>5,†</sup>  
P.E. Garrett,<sup>6</sup> K. Hadyńska-Klęk,<sup>7</sup> A. Goasduff,<sup>8,9</sup> D. Testov,<sup>8,‡</sup> S.D. Bakes,<sup>4,9,10</sup> D. Bazzacco,<sup>8,9</sup>  
G. Benzoni,<sup>11</sup> T. Berry,<sup>4</sup> D. Brugnara,<sup>9,10</sup> F. Camera,<sup>11,12</sup> W.N. Catford,<sup>4</sup> M. Chiari,<sup>1</sup>  
F. Galtarossa,<sup>10</sup> N. Gelli,<sup>1</sup> A. Gottardo,<sup>10</sup> A. Gozzelino,<sup>10</sup> A. Illana,<sup>10,§</sup> J. Keatings,<sup>13</sup> D. Mengoni,<sup>8,9</sup>  
L. Morrison,<sup>4</sup> D.R. Napoli,<sup>10</sup> M. Ottanelli,<sup>1</sup> P. Ottanelli,<sup>1,2</sup> G. Pasqualato,<sup>8,9</sup> F. Recchia,<sup>8,9</sup>  
S. Riccetto,<sup>14,15,¶</sup> M. Scheck,<sup>13</sup> M. Siciliano,<sup>9,10</sup> J.J. Valiente Dóbon,<sup>10</sup> and I. Zanon<sup>9,10</sup>

<sup>1</sup>*INFN Sezione di Firenze, I-50019 Firenze, Italy*

<sup>2</sup>*Dipartimento di Fisica e Astronomia, Università degli Studi di Firenze, I-50019 Firenze, Italy*

<sup>3</sup>*IRFU, CEA, Université Paris-Saclay, F-91191 Gif-sur-Yvette, France*

<sup>4</sup>*School of Mathematics and Physics, University of Surrey, GU2 7XH Guildford, United Kingdom*

<sup>5</sup>*Grand Accélérateur National d'Ions Lourds, CEA/DRF-CNRS/IN2P3, F-14076 Caen, France*

<sup>6</sup>*Department of Physics, University of Guelph, N1G 2W1 Guelph, Canada*

<sup>7</sup>*Heavy Ion Laboratory, University of Warsaw, PL-02-093 Warszawa, Poland*

<sup>8</sup>*INFN Sezione di Padova, I-35131 Padova, Italy*

<sup>9</sup>*Dipartimento di Fisica e Astronomia, Università degli Studi di Padova, I-35131 Padova, Italy*

<sup>10</sup>*INFN Laboratori Nazionali di Legnaro, I-35020 Padova, Italy*

<sup>11</sup>*INFN Sezione di Milano, I-20133 Milano, Italy*

<sup>12</sup>*Dipartimento di Fisica, Università di Milano, I-20133 Milano, Italy*

<sup>13</sup>*Department of Physics, University of West of Scotland, G72 0LH Paisley, United Kingdom*

<sup>14</sup>*Dipartimento di Fisica e Geologia, Università degli Studi di Perugia, I-06123 Perugia, Italy*

<sup>15</sup>*INFN Sezione di Perugia, I-06123 Perugia, Italy*

(Dated: August 14, 2024)

Low-lying states of  $^{94}\text{Zr}$  were investigated via low-energy multi-step Coulomb excitation. From the measured  $\gamma$ -ray yields, 13 reduced transition probabilities between low-spin states were determined, together with the spectroscopic quadrupole moments of the  $2^+_{1,2}$  states. Based on this information, for the first time in the Zr isotopic chain, the shapes of the  $0^+_{1,2}$  states including their deformation softness were inferred in a model-independent way using the quadrupole sum rules approach. The ground state of  $^{94}\text{Zr}$  possesses a rather diffuse shape associated with a spherical configuration, while the  $0^+_2$  state is oblate and more strongly deformed. The observed features of shape coexistence in  $^{94}\text{Zr}$  are in agreement with Monte-Carlo shell-model predictions, and the present results are vital to refine the IBM-CM description of the Zr isotopes around  $A \approx 100$  in terms of an intertwined quantum phase transition.

In the nuclear landscape characterized by gently evolving ground-state properties, the region of strontium and zirconium nuclei with neutron number  $N$  close to 60 stands out. Nowhere else is the transition from a spherical to a strongly deformed ground state occurring as rapidly as when passing from  $N = 58$   $^{96}\text{Sr}$ ,  $^{98}\text{Zr}$  to  $N = 60$   $^{98}\text{Sr}$ ,  $^{100}\text{Zr}$  [1–3], and a reproduction of this unique behaviour had been a long-standing challenge for nuclear-structure theory [4–12]. This dramatic shape change is often interpreted as a quantum phase transition (QPT) [13, 14], in analogy to more familiar thermodynamic phase changes seen in many macroscopic systems. The transition from one shape phase to another corresponds to structural rearrangements in the nucleus, which are reflected in observables such as, e.g., two-nucleon separation energies, charge radii, level energies, and transition rates (see, e.g., Refs. [15–20]).

Recently, two theoretical approaches [21–24] succeeded to describe the abrupt change in deformation observed at  $N = 58 - 60$  in the Zr isotopic chain, both of them invoking the QPT concept. The Monte-Carlo shell-model (MCSM) calculations [21] attributed the shape

transition to the so-called type-II shell evolution mechanism [25, 26], being an example of self-organization of macroscopic systems observed in many domains of physics and beyond [27]. This mechanism involves modifications of nuclear effective single-particle energies due to the occupation of specific orbitals. In the Zr nuclei, tensor and central forces act coherently to substantially lower the energies of proton-neutron spin-orbit partners, closing the pronounced spherical subshell gaps. The reorganized subshell sequence favors larger deformation thanks to coherent contributions of the configurations involved (Jahn-Teller effect [28]). According to the MCSM calculations, the deformed configurations assume a variety of shapes throughout the Zr isotopic chain that include prolate, oblate and triaxial ones [21].

A large set of experimental spectroscopic data related to the shape transition in the Zr isotopes was also satisfactorily reproduced in the framework of configuration mixing within the interacting boson model (IBM-CM) [22–24]. With the IBM-CM, another QPT of shape-evolution was identified in the Zr intruder configuration, on top of the QPT in the configuration con-

tent of the ground state also suggested by MCSM [21]. This evolution in structure was dubbed as *intertwined* QPT (IQPT) [24]. In an IQPT, two configurations are present, each of which may undergo an individual QPT. For  $N < 60$ , the IBM-CM calculations of Ref. [24] predict a spherical vibrational (possessing good U(5) symmetry) configuration for the ground state, coexisting with a weakly deformed (quasi-U(5) symmetry) intruder configuration. The two configurations interchange at  $N = 60$ , and in parallel the intruder configuration undergoes a QPT from weakly deformed to well deformed (good rotational SU(3) symmetry). Similar to the MCSM calculations, the IBM-CM reproduces the observed small mixing [29] between the normal and intruder configurations.

While the experimental information on the nature of  $0_2^+$  states in the Zr isotopes with  $N \geq 60$  [30–33] is limited due to the neutron-rich character and short half-lives of the nuclei in question, definitive conclusions regarding their character in  $N < 60$  Zr nuclei are not possible either. For example, the results of lifetime measurements for excited states in  $^{98}\text{Zr}$  [34] were interpreted, with a guidance from MCSM calculations, in terms of triple shape coexistence with notably a moderately deformed  $0_2^+$  state and a rotational structure built on it. At the same time, a different set of lifetimes [35] measured in the same nucleus was found to be in general agreement with a vibrational interpretation of states built on the  $0_2^+$  state. Both theoretical approaches, however, do not reproduce the large  $B(E2; 4_1^+ \rightarrow 2_2^+)$  value deduced from the data [34, 35]. Moreover, in  $^{94,96}\text{Zr}$  enhanced  $B(E2; 2_2^+ \rightarrow 0_2^+)$  values of 19(2) W.u. [36] and 36(11) W.u. [29], respectively, were determined and interpreted as corresponding to in-band transitions in collective rotational structures built on the deformed  $0_2^+$  states, thus supporting a shape-coexistence scenario. However, a subsequent reevaluation [37] of the existing experimental data for  $^{96}\text{Zr}$  showed that a vibrational character of the structure built on the  $0_2^+$  state cannot be excluded.

The above examples show the limitations of the current experimental knowledge of the even-even Zr nuclei and the difficulties in distinguishing between various interpretations. In particular, the MCSM results tend to be presented in the context of the underlying shapes, which can only be deduced from the existing experimental data using strong model assumptions. Critical data, such as spectroscopic quadrupole moments,  $Q_s$ , of  $2^+$  states that could discriminate between a spherical-vibrational and deformed-rotational interpretation, have been lacking.

The present Letter reports not only the determination of  $Q_s$  for the  $2_1^+$  and  $2_2^+$  states, but further provides model-independent quantities  $\langle Q^2 \rangle$  and  $\langle Q^3 \cos 3\delta \rangle$ , which are representative of the nuclear shape, determined for the  $0_1^+$  and  $0_2^+$  states in  $^{94}\text{Zr}$  in a multi-step Coulomb-excitation study. These experimental results establish coexistence of a quasi-spherical ground state and a more

deformed oblate structure built on the  $0_2^+$  state, and are compared with new IBM-CM calculations building on those reported in Ref. [24], as well as with the MCSM calculations [3, 21].

The Coulomb-excitation technique is ideally suited to study collectivity of yrast and non-yrast states at low spin and excitation energy [38]. The  $^{94}\text{Zr}$  nucleus was chosen among the Zr isotopes since it has a favorable level scheme with the states of interest below 2.5 MeV excitation energy. Moreover, the relatively large  $B(E2; 0_2^+ \rightarrow 2_1^+) = 9.3(4)$  W.u. value [36] results in an enhanced cross section to Coulomb excite the  $0_2^+$  state via a two-step process, facilitating population of higher-lying states. Furthermore, high-intensity beams of the stable  $^{94}\text{Zr}$  can be produced, leading to data sets with high statistical quality.

The experiment was performed at the INFN Legnaro National Laboratories (LNL). During 4 days of data taking, a 0.1-pnA beam of  $^{94}\text{Zr}$  impinged on a 0.97(2)-mg/cm<sup>2</sup> thick, self-supporting  $^{208}\text{Pb}$  target (the target thickness was measured at the INFN LABEC laboratory using the Rutherford back-scattering technique [39]). The beam energy, 370 MeV, fulfilled Cline’s “safe”-energy criterion [40] for the range of scattering angles observed, ensuring that the contribution from the nuclear forces to the excitation process was negligible. The  $\gamma$  rays deexciting the populated states were detected by the GALILEO  $\gamma$ -ray spectrometer [41] combined with six large-volume  $3'' \times 3''$  LaBr<sub>3</sub>:Ce detectors [42], and the scattered  $^{94}\text{Zr}$  ions by the SPIDER silicon array [43]. The absolute photo-peak efficiencies at 1332.5 keV of GALILEO and the LaBr<sub>3</sub>:Ce array were 2.1% and 1.1%, respectively. SPIDER comprised seven silicon detectors with trapezoidal shapes, segmented eight-fold in polar angle and covering  $\theta_{LAB}$  angles from 123° to 161°. The standard GALILEO and SPIDER presorting and data-correction procedures [41, 43, 44] were implemented in the analysis, resulting in 8.7 keV full width at half maximum at 919 keV energy in the final Doppler-corrected  $\gamma$ -ray spectrum from GALILEO in coincidence with the back-scattered  $^{94}\text{Zr}$  ions. This spectrum is shown in Fig. 1, while Fig. 2 reports a partial  $^{94}\text{Zr}$  level scheme indicating the transitions observed in the present work. The inset of Fig. 1 displays the  $2_2^+ \rightarrow 0_2^+$  transition that was only observed in the  $\gamma$ - $\gamma$ -particle coincidence analysis combining the HPGe and LaBr<sub>3</sub>:Ce data, confirming its placement proposed in Ref. [36]. In addition to transitions in  $^{94}\text{Zr}$ , a few weaker lines in the spectrum, at the level of 0.3% or less of the intensity of the  $2_1^+ \rightarrow 0_1^+$   $^{94}\text{Zr}$  transition, arise from sub-barrier one-neutron transfer to  $^{95}\text{Zr}$ . The  $^{95}\text{Zr}$  levels identified correspond to those with the largest spectroscopic factors for one-neutron transfer [45], and the observed populations are in line with the transfer cross sections measured in, e.g., Ref. [46] for conditions in which the nuclear interaction had a negligible influence on the excitation process.

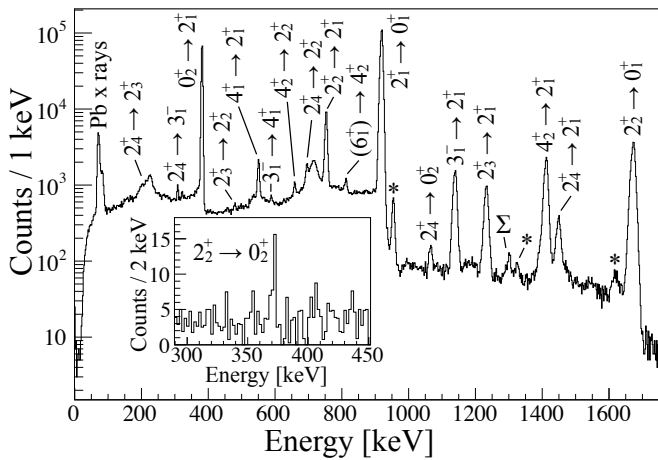


FIG. 1. Portion of the  $\gamma$ -ray energy spectrum observed following Coulomb excitation of the  $^{94}\text{Zr}$  beam impinging on a  $^{208}\text{Pb}$  target, Doppler corrected for the projectile. Transitions in  $^{95}\text{Zr}$  are marked with asterisks and  $\Sigma$  denotes a sum peak. The inset shows the  $2_2^+ \rightarrow 0_2^+$  transition observed in  $\gamma$ - $\gamma$ -particle coincidences (gated on the  $0_2^+ \rightarrow 2_1^+$   $\gamma$ -ray transition).

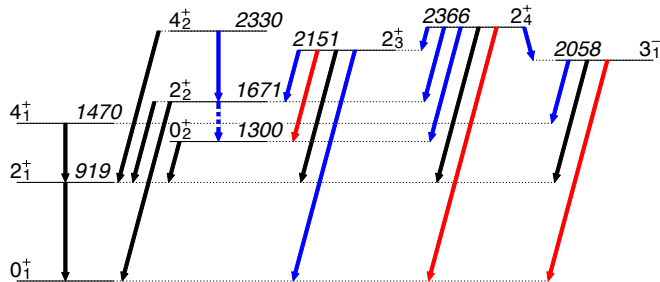


FIG. 2. Partial level scheme of  $^{94}\text{Zr}$  showing transitions relevant for the present work. The level energies are given in keV. The number of counts observed for the transitions marked in black was sufficient to subdivide the data into eight angular ranges. For the transitions marked in blue, the total number of counts in coincidence with the SPIDER array was used in the analysis. The  $2_2^+ \rightarrow 0_2^+$  transition was observed only in  $\gamma$ - $\gamma$ -particle coincidences (dashed blue). Transitions marked in red have not been observed in the present experiment, but the corresponding matrix elements were considered in the data analysis with the GOSIA code.

The extracted numbers of  $\gamma$ -particle coincidences for the observed transitions in  $^{94}\text{Zr}$  were analyzed using the GOSIA code [47]. The measured yields were divided into the eight angular ranges defined by the SPIDER segmentation [43] to exploit the angular dependence of the Coulomb-excitation cross sections, except for weaker transitions for which the coincidences with the entire SPIDER array were considered (see Fig. 2). While the present experiment was insensitive to  $B(M1)$  and  $B(E1)$  values, the corresponding matrix elements were included in the multidimensional GOSIA fit together with those for  $E2$  and  $E3$  multipolarities, and their values were constrained by complementary spectroscopic data. The level

lifetimes were taken from Refs. [36, 48], the  $E2/M1$  mixing ratios from Ref. [49], and the branching ratios from Refs. [36, 49–51]. The final set of matrix elements obtained in the analysis reproduces all these values within  $\pm 1\sigma$  uncertainty. Moreover, the level scheme considered in the fit was extended to higher excitation energy to account for possible excitations of unobserved states, and observation upper limits were imposed constraining the unobserved  $2_3^+ \rightarrow 0_2^+$  and  $2_4^+ \rightarrow 0_1^+$  transitions, for which branching ratios are unknown. The intensity of the  $(6_1^+) \rightarrow 4_2^+$  transition has been included in the analysis, but due to ambiguities [49, 50, 52] regarding the spin of the presumed  $(6_1^+)$  state at 3142 keV, the corresponding matrix element is not reported. Absolute normalization of the measured cross sections was achieved via inclusion in the fit of a weighted average of the  $2_1^+$  lifetimes [53–55] and consequently the analysis was not sensitive to the  $B(E2; 2_1^+ \rightarrow 0_1^+)$  value [38, 56]. The following sign convention was imposed for  $E2$  matrix elements: those for in-band transitions were assumed to be positive, as well as those of  $\langle 0_2^+ || E2 || 2_1^+ \rangle$ ,  $\langle 2_1^+ || E2 || 2_3^+ \rangle$  and  $\langle 2_1^+ || E2 || 2_4^+ \rangle$ , with the signs of remaining matrix elements determined relative to them.

The present work determined  $Q_s$  of the  $2_{1,2}^+$  states in  $^{94}\text{Zr}$  (Table I) – the first such determination in the Zr isotopic chain [57]. Moreover, a large number of  $E2$  matrix elements were precisely measured that are reported in Table II together with the corresponding  $B(E2)$  values. In addition, the  $B(E3; 3_1^- \rightarrow 0_1^+) = 33(3)$  W.u. value was extracted from the data, which agrees with the evaluated value [58], but is considerably more precise.

TABLE I. Diagonal  $E2$  matrix elements measured in the present work and corresponding spectroscopic quadrupole moments, compared with those resulting from IBM-CM calculations.

$J_i$	$\langle J_i    E2    J_i \rangle$ [eb]	$Q_s(J_i)$ [eb]	
	Exp.	Exp.	IBM-CM
$2_1^+$	$+0.131_{-0.030}^{+0.013}$	$+0.099_{-0.025}^{+0.010}$	+0.066
$2_2^+$	+0.37(4)	+0.28(3)	+0.31

The different deformations of two structures in  $^{94}\text{Zr}$  are evidenced by the large difference between the spectroscopic quadrupole moments measured for the  $2_{1,2}^+$  states (Table I). To get more precise, model-independent information on the nuclear charge distribution in the ground state and the first excited  $0^+$  state, a quadrupole sum rule analysis [38, 40, 59] was applied to the obtained set of  $E2$  matrix elements. Since the  $E2$  operator is a spherical tensor, its products coupled to zero angular momentum are rotationally invariant. Hence, their expectation values can be expressed on one hand using charge distribution parameters defined in the intrinsic frame of the nucleus, and on the other using combinations of  $E2$  matrix

TABLE II. Transitional  $E2$  matrix elements obtained in the present work (with the exception of  $\langle 0_1^+ || E2 || 2_1^+ \rangle$  provided for completeness) and corresponding  $B(E2)$  values compared with those resulting from IBM-CM calculations.

$J_i \rightarrow J_f$	$\langle J_f    E2    J_i \rangle$ [eb]	$B(E2; J_i \rightarrow J_f)$ [W.u.]	
	Exp.	Exp.	IBM-CM
$2_1^+ \rightarrow 0_1^+$	+0.250(7) <sup>ab</sup>	4.8(2) <sup>b</sup>	2.7
$0_2^+ \rightarrow 2_1^+$	+0.155(4) <sup>a</sup>	9.5(5)	9.3
$4_1^+ \rightarrow 2_1^+$	+0.141(4) <sup>a</sup>	0.87(5)	— <sup>c</sup>
$2_2^+ \rightarrow 0_2^+$	+0.484(12) <sup>a</sup>	18.5(9)	20.2
$2_2^+ \rightarrow 2_1^+$	+0.03(3)	< 0.3	1.49
$2_2^+ \rightarrow 0_1^+$	+0.221(6)	3.9(2)	0.82
$4_2^+ \rightarrow 2_2^+$	+0.96(3) <sup>a</sup>	40(3)	26.6
$4_2^+ \rightarrow 2_1^+$	+0.607(16)	16.1(9)	2.1
$2_3^+ \rightarrow 2_2^+$	+0.249 <sup>+0.019</sup> <sub>-0.040</sub>	4.9 <sup>+0.7</sup> <sub>-1.6</sub>	17.3
$2_3^+ \rightarrow 0_2^+$	< 0.13 <sup>d</sup>	< 1.3	0.07
$2_3^+ \rightarrow 2_1^+$	+0.290 <sup>+0.014a</sup> <sub>-0.012</sub>	6.6 <sup>+0.6</sup> <sub>-0.5</sub>	1.2
$2_3^+ \rightarrow 0_1^+$	-0.0182 <sup>+0.0016</sup> <sub>-0.0020</sub>	0.026 <sup>+0.005</sup> <sub>-0.006</sub>	0.001
$2_4^+ \rightarrow 2_3^+$	-0.02 <sup>+0.06</sup> <sub>-0.03</sub>	< 0.2	2.44
$2_4^+ \rightarrow 2_2^+$	$\pm 0.073$ <sup>+0.030</sup> <sub>-0.018</sub>	0.4 <sup>+0.3</sup> <sub>-0.2</sub>	0.1
$2_4^+ \rightarrow 0_2^+$	$\pm 0.177$ <sup>+0.010</sup> <sub>-0.005</sub>	2.47 <sup>+0.30</sup> <sub>-0.14</sub>	0.06
$2_4^+ \rightarrow 2_1^+$	+0.092 <sup>+0.006a</sup> <sub>-0.004</sub>	0.67 <sup>+0.09</sup> <sub>-0.06</sub>	0.001
$2_4^+ \rightarrow 0_1^+$	-0.001 <sup>+0.003</sup> <sub>-0.006</sub>	< 4 · 10 <sup>-3</sup>	3 · 10 <sup>-4</sup>

<sup>a</sup> Sign imposed in the analysis (see text for details).

<sup>b</sup> Determined from literature data.

<sup>c</sup> Outside IBM-CM model space (see Ref. [24] for details).

<sup>d</sup> Positive sign determined.

elements measured in the laboratory frame. The first-order invariant  $\langle Q^2 \rangle$ , related to the overall deformation, is constructed from the squares of  $E2$  matrix elements connecting the  $0^+$  state of interest to all  $2^+$  states. The second-order invariant  $\langle Q^3 \cos(3\delta) \rangle$  involves triple products of transitional and diagonal  $E2$  matrix elements and thus requires the knowledge of  $2^+$  quadrupole moments with their absolute sign, and relative signs of transitional matrix elements. The quantity  $\langle \delta \rangle$  indicates the degree of non-axiality. Specifically,  $\langle \cos(3\delta) \rangle$  is +1 for a prolate shape ( $\langle \delta \rangle = 0^\circ$ ), 0 for a maximally triaxial shape ( $\langle \delta \rangle = 30^\circ$ ), and -1 for an oblate shape ( $\langle \delta \rangle = 60^\circ$ ). Moreover, the third-order invariant  $\langle Q^4 \rangle$  was determined from the experimental  $E2$  matrix elements, providing information on the variance of the  $\langle Q^2 \rangle$  invariant. This quantity, defined as  $\sigma(Q^2) = \sqrt{\langle Q^4 \rangle - (\langle Q^2 \rangle)^2}$ , is related to softness in the overall deformation.

The results of this approach are presented in Table III and Fig. 3. The  $\langle Q^2 \rangle$  of the  $0_2^+$  state is  $\approx 2.7$  times larger than that of the  $0_1^+$  state. However, the fact that

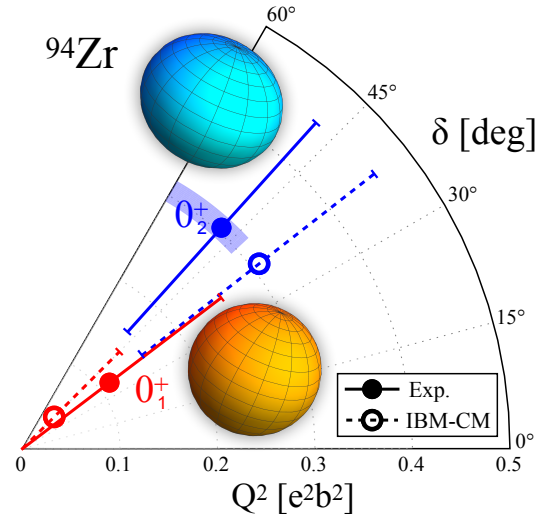


FIG. 3. Shape parameters for the  $0_{1,2}^+$  states in the  $(Q^2, \delta)$  plane resulting from the sum-rules analysis. The experimental results are shown with full circles, while the shaded areas represent their uncertainties (for the  $0_1^+$  state the respective area is smaller than the marker size). The results of the IBM-CM calculations are shown with empty circles. The lines (solid for the experimental values and dashed for the IBM-CM calculations) represent  $\sigma(Q^2)$  dispersions. The results are reported in red for the  $0_1^+$  state and in blue for the  $0_2^+$  state. The illustrative shapes are plotted using  $\beta_2$  and  $\gamma$  values derived from the experimental invariant quantities for the  $0_2^+$  state (blue ellipsoid), and  $\beta_2 = 0$  for the  $0_1^+$  state (orange sphere), see text for details.

the dispersion of  $\langle Q^2 \rangle$  for the  $0_1^+$  state is comparable with the  $\langle Q^2 \rangle$  value itself indicates that the ground state of  $^{94}\text{Zr}$  exhibits fluctuations about a spherical shape. In contrast,  $\sigma(Q^2)$  for the  $0_2^+$  state is considerably smaller than  $\langle Q^2 \rangle$ , which suggests a moderate static deformation. More insight into the shape of the  $0_2^+$  state can be obtained from its value of  $\langle \cos(3\delta) \rangle$  (equivalent to  $\langle \delta \rangle = 48$ <sup>+12</sup><sub>-5</sub>°), which indicates an oblate deformation with a possible degree of triaxiality, consistent with the positive value of the  $2_2^+$  spectroscopic quadrupole moment. For the  $0_1^+$  state, the  $\langle \cos(3\delta) \rangle$  value is of limited relevance since  $\sigma(Q^2) > \langle Q^2 \rangle$ .

TABLE III. Results of the quadrupole sum-rules analysis of experimental  $E2$  matrix elements obtained in the present work (Exp.) compared with IBM-CM calculations (Th.).

$J_i$	$\langle Q^2 \rangle$ [ $e^2b^2$ ]		$\sigma(Q^2)$ [ $e^2b^2$ ]		$\langle \cos(3\delta) \rangle$	
	Exp.	Th.	Exp.	Th.	Exp.	Th.
$0_1^+$	0.112(4)	0.046	0.143(4)	0.094	-0.37(7)	-0.72
$0_2^+$	0.305(12)	0.308	0.14(3)	0.153	-0.8(2)	-0.4

The experimental results were compared with IBM-CM calculations building on Ref. [24]. Using the  $Q_s(2_{1,2}^+)$

values measured in the present work it was possible to fix the  $\chi$  model parameter to  $\chi = +0.6$  instead of the previously adopted  $\chi = -0.6$ . This choice does not change the spectrum reported in Ref. [24] but is responsible for the prolate-oblate nature of the deformation. The calculated  $B(E2)$  values are shown in Table II. The overall agreement is satisfactory, except for the  $B(E2; 4_2^+ \rightarrow 2_1^+)$  and  $B(E2; 2_3^+ \rightarrow 2_2^+)$  values. For the former, the discrepancy could occur due to mixing between the  $4_2^+$  and  $4_1^+$  states, the latter being outside the IBM-CM model space [24]. The calculated spectroscopic quadrupole moments, reported in Table I, are also in satisfactory agreement with the experimental results, with a much larger value predicted for the  $2_2^+$  state with respect to the  $2_1^+$  state.

The results of the quadrupole sum rules analysis within the IBM-CM are reported in Table III and shown in Fig. 3. The calculated  $\langle Q^2 \rangle$  invariant for the  $0_1^+$  state is slightly smaller than the experimental one, mainly because of the smaller calculated  $B(E2; 2_1^+ \rightarrow 0_1^+)$  value (see Table II). However, both the experimental and theoretical  $\langle Q^2 \rangle$  results provide a consistent picture of a quasi-spherical ground state exhibiting large quantum fluctuations in the overall deformation. The calculated and experimental  $\langle Q^2 \rangle$  invariants for the  $0_2^+$  state are in good agreement. For the  $\langle \cos(3\delta) \rangle$  observable the IBM-CM yields the same sign (oblate) as the experimental results. In both cases, the results translate to very similar  $\langle \delta \rangle$  values (see Fig. 3).

To enable comparison with other calculations, it is possible to derive from the model-independent quantities  $\langle Q^2 \rangle$  and  $\langle Q^3 \cos(3\delta) \rangle$  the usual deformation parameters  $\beta_2$  and  $\gamma^1$ . The results show that the shapes obtained from the present experimental and IBM-CM results are also in agreement with those predicted by the MCSM [3, 21]: the *T-plot* analysis for  $^{94}\text{Zr}$  [3] indicates that the ground state is spherical, and the  $0_2^+$  state is oblate deformed with  $\beta_2 \lesssim 0.2$  (as compared to  $\langle \beta_2 \rangle = 0.194(4)$  resulting from the current experimental data) and a  $\gamma$  value similar to those deduced here.

To summarize, this work reports the first experimental determination of shape parameters and their dispersions in a Zr isotope using quadrupole sum rules. The procedure, applied to the ground state and the first excited  $0^+$  state in  $^{94}\text{Zr}$ , involved notably a measurement of spectroscopic quadrupole moments of the  $2_{1,2}^+$  states, which represents a level of detail that is unique in the Zr nuclei. The rotational invariants obtained from the experimentally determined  $E2$  matrix elements establish conclusively shape-coexisting structures in  $^{94}\text{Zr}$ , revealing a ground state with a shape that is not well defined, but tends towards sphericity, and a  $0_2^+$  state being more

deformed and oblate shaped. The invariants calculated within the IBM-CM model agree with the experimental findings and are also consistent with MCSM predictions for both states in question, supporting the QPT (IQPT) picture for a nucleus with  $N < 60$ . Reaching a similar level of detail at  $N = 60$  and beyond will represent a challenge for new-generation radioactive-ion beam facilities.

The authors thank the staff of the LNL Tandem-XTU accelerator for the excellent quality of the  $^{94}\text{Zr}$  beam, and M. Loriggiola for producing the  $^{208}\text{Pb}$  target. The use of germanium detectors from GAMMAPOOL is acknowledged. This work was supported in part by the Natural Sciences and Engineering Research Council (Canada).

---

\* naomi.marchini@fi.infn.it

† noam.gavriellov@ganil.fr

‡ Present address: Extreme Light Infrastructure-Nuclear Physics (ELI-NP), National Institute for Physics and Nuclear Engineering “Horia Hulubei”, 077125 Măgurele-Bucharest, Romania

§ Present address: Grupo de Física Nuclear (GFN) and IPARCOS, Universidad Complutense de Madrid, CEI Moncloa, E-28040 Madrid, Spain

¶ Present address: Department of Physics, Queen’s University, ON K7L 3N6 Kingston, Canada

- [1] P. Campbell, I. Moore, and M. Pearson, *Prog. Part. Nucl. Phys.* **86**, 127 (2016).
- [2] P. E. Garrett, M. Zielińska, and E. Clément, *Prog. Part. Nucl. Phys.* **124**, 103931 (2022).
- [3] S. Leoni, B. Fornal, A. Bracco, Y. Tsunoda, and T. Otsuka, *Prog. Part. Nucl. Phys.*, 104119 (2024).
- [4] P. Federman and S. Pittel, *Phys. Rev. C* **20**, 820 (1979).
- [5] J. Skalski, P.-H. Heenen, and P. Bonche, *Nucl. Phys. A* **559**, 221 (1993).
- [6] C. Özen and D. Dean, *Phys. Rev. C* **73**, 014302 (2006).
- [7] K. Sieja, F. Nowacki, K. Langanke, and G. Martínez-Pinedo, *Phys. Rev. C* **79**, 064310 (2009).
- [8] R. Rodríguez-Guzmán, P. Sarriguren, L. Robledo, and S. Perez-Martin, *Phys. Lett. B* **691**, 202 (2010).
- [9] H. Mei, J. Xiang, J. M. Yao, Z. P. Li, and J. Meng, *Phys. Rev. C* **85**, 034321 (2012).
- [10] A. Petrovici, *Phys. Rev. C* **85**, 034337 (2012).
- [11] J. Xiang, Z. Li, Z. Li, J. Yao, and J. Meng, *Nucl. Phys. A* **873**, 1 (2012).
- [12] K. Nomura, R. Rodríguez-Guzmán, and L. M. Robledo, *Phys. Rev. C* **94**, 044314 (2016).
- [13] P. Cejnar, J. Jolie, and R. F. Casten, *Rev. Mod. Phys.* **82**, 2155 (2010).
- [14] L. Fortunato, *Prog. Part. Nucl. Phys.* **121**, 103891 (2021).
- [15] S. A. Johansson, *Nucl. Phys.* **64**, 147 (1965).
- [16] E. Cheifetz, R. Jared, S. Thompson, and J. Wilhelm, *Phys. Rev. Lett.* **25**, 38 (1970).
- [17] H. Thayer, J. Billowes, P. Campbell, P. Dendooven, K. Flanagan, D. Forest, J. Griffith, J. Huikari, A. Jokinen, R. Moore, *et al.*, *J. Phys. G: Nucl. Part. Phys.* **29**, 2247 (2003).

---

<sup>1</sup>  $\langle \beta_2 \rangle = (\frac{3}{4\pi} ZR^2)^{-1} \cdot \sqrt{\langle Q^2 \rangle}$ , where  $R = 1.2A^{1/3}$  [fm], and  $\langle \gamma \rangle = \langle \delta \rangle$  [38]. For  $^{94}\text{Zr}$ ,  $\langle \beta_2 \rangle \approx 0.35\sqrt{\langle Q^2 \rangle}$ .

- [18] S. Ansari, J.-M. Régis, J. Jolie, N. Saed-Samii, N. Warr, W. Korten, M. Zielińska, M.-D. Salsac, A. Blanc, M. Jentschel, *et al.*, *Phys. Rev. C* **96**, 054323 (2017).
- [19] M. Wang, W. Huang, F. Kondev, G. Audi, and S. Naimi, *Chinese Phys. C* **45**, 030003 (2021).
- [20] G. Pasqualato, S. Ansari, J. Heines, V. Modamio, A. Görge, W. Korten, J. Ljungvall, E. Clément, J. Dudoet, A. Lemasson, *et al.*, *Eur. Phys. J. A* **59**, 276 (2023).
- [21] T. Togashi, Y. Tsunoda, T. Otsuka, and N. Shimizu, *Phys. Rev. Lett.* **117**, 172502 (2016).
- [22] J. E. García-Ramos and K. Heyde, *Phys. Rev. C* **100**, 044315 (2019).
- [23] J. E. García-Ramos and K. Heyde, *Phys. Rev. C* **102**, 054333 (2020).
- [24] N. Gavrielov, A. Leviatan, and F. Iachello, *Phys. Rev. C* **105**, 014305 (2022).
- [25] T. Otsuka and Y. Tsunoda, *J. Phys. G: Nucl. Part. Phys.* **43**, 024009 (2016).
- [26] T. Otsuka, Y. Tsunoda, T. Togashi, N. Shimizu, and T. Abe, in *J. Phys.: Conf. Ser.*, Vol. 966 (IOP Publishing, 2018) p. 012027.
- [27] H. Haken, *Synergetics* (Springer Berlin, Heidelberg, 1983).
- [28] H. Jahn and E. Teller, *Proc. R. Soc. A* **161**, 2020 (1937).
- [29] C. Kremer, S. Aslanidou, S. Bassauer, M. Hilcker, A. Krugmann, P. von Neumann-Cosel, T. Otsuka, N. Pietralla, V. Y. Ponomarev, N. Shimizu, *et al.*, *Phys. Rev. Lett.* **117**, 172503 (2016).
- [30] H. Mach, M. Moszyński, R. Gill, F. Wahn, J. Winger, J. Hill, G. Molnár, and K. Sistemich, *Phys. Lett. B* **230**, 21 (1989).
- [31] W. Urban, T. Rząca-Urban, J. Wiśniewski, I. Ahmad, A. G. Smith, and G. S. Simpson, *Phys. Rev. C* **99**, 064325 (2019).
- [32] J. Wu, M. P. Carpenter, F. G. Kondev, R. V. F. Janssens, S. Zhu, E. A. McCutchan, A. D. Ayangeakaa, J. Chen, J. Clark, D. J. Hartley, T. Lauritsen, N. Pietralla, G. Savard, D. Seweryniak, and V. Werner, *Phys. Rev. C* **109**, 024314 (2024).
- [33] J. Hill, D. Schwellenbach, F. Wahn, J. Winger, R. Gill, H. Ohm, and K. Sistemich, *Phys. Rev. C* **43**, 2591 (1991).
- [34] P. Singh, W. Korten, T. W. Hagen, A. Görge, L. Grente, M.-D. Salsac, F. Farget, E. Clément, G. de France, T. Braunroth, *et al.*, *Phys. Rev. Lett.* **121**, 192501 (2018).
- [35] V. Karayonchev, J. Jolie, A. Blazhev, A. Dewald, A. Esmaylzadeh, C. Fransen, G. Häfner, L. Knafla, J. Litzinger, C. Müller-Gatermann, *et al.*, *Phys. Rev. C* **102**, 064314 (2020).
- [36] A. Chakraborty, E. Peters, B. Crider, C. Andreoiu, P. Bender, D. Cross, G. Demand, A. Garnsworthy, P. Garrett, G. Hackman, *et al.*, *Phys. Rev. Lett.* **110**, 022504 (2013).
- [37] W. Witt, N. Pietralla, V. Werner, and T. Beck, *Eur. Phys. J. A* **55**, 1 (2019).
- [38] M. Zielińska, Low-energy Coulomb excitation and nuclear deformation, in *The Euroscool on Exotic Beams, Vol. VI*, edited by S. M. Lenzi and D. Cortina-Gil (Springer International Publishing, Cham, 2022) pp. 43–86.
- [39] M. Rocchini, M. Chiari, E. Pasquali, A. Nannini, K. Hadyńska-Klęk, P. Sona, D. Bazzacco, G. Benzoni, F. Camera, C. Czelusniak, *et al.*, *Nucl. Instrum. Methods Phys. Res. B* **486**, 68 (2021).
- [40] D. Cline, *Ann. Rev. Nucl. Part. Sci.* **36**, 683 (1986).
- [41] A. Goasduff, D. Mengoni, F. Recchia, J. Valiente-Dobón, R. Menegazzo, G. Benzoni, D. Barrientos, M. Bellato, N. Bez, M. Biasotto, *et al.*, *Nucl. Instrum. Methods Phys. Res. A* **1015**, 165753 (2021).
- [42] A. Giaz, L. Pellegri, S. Riboldi, F. Camera, N. Blasi, C. Boiano, A. Bracco, S. Brambilla, S. Ceruti, S. Coelli, *et al.*, *Nucl. Instrum. Methods Phys. Res. A* **729**, 910 (2013).
- [43] M. Rocchini, K. Hadyńska-Klęk, A. Nannini, J. Valiente-Dobón, A. Goasduff, D. Testov, D. Mengoni, P. John, M. Siciliano, B. Melon, *et al.*, *Nucl. Instrum. Methods Phys. Res. A* **971**, 164030 (2020).
- [44] M. Rocchini, K. Hadyńska-Klęk, A. Nannini, A. Goasduff, M. Zielińska, D. Testov, T. Rodríguez, A. Gargano, F. Nowacki, G. De Gregorio, *et al.*, *Phys. Rev. C* **103**, 014311 (2021).
- [45] C. R. Bingham and G. T. Fabian, *Phys. Rev. C* **7**, 1509 (1973).
- [46] W. Kernan, C. Wu, X. Liu, X. Han, D. Cline, T. Czosnyka, M. Guidry, M. Halbert, S. Juutinen, A. Kavka, R. Kincaid, J. Rasmussen, S. Sorensen, M. Stoyer, and E. Vogt, *Nucl. Phys. A* **524**, 344 (1991).
- [47] T. Czosnyka, D. Cline, and C. Wu, *Bull. Am. Phys. Soc.* **28**, 745 (1983).
- [48] E. Peters, A. Chakraborty, B. Crider, B. Davis, M. Gnanamani, M. McEllistrem, F. Prados-Estévez, J. Vanhoy, and S. Yates, *Phys. Rev. C* **88**, 024317 (2013).
- [49] E. Elhami, J. Orce, M. Scheck, S. Mukhopadhyay, S. Choudry, M. McEllistrem, S. Yates, C. Angell, M. Boswell, B. Fallin, *et al.*, *Phys. Rev. C* **78**, 064303 (2008).
- [50] N. Fotiades, J. Cizewski, J. Becker, L. Bernstein, D. McNabb, W. Younes, R. Clark, P. Fallon, I. Lee, A. Macchiavelli, *et al.*, *Phys. Rev. C* **65**, 044303 (2002).
- [51] B. Singh, H. Taylor, and P. Tivin, *J. Phys. G: Nucl. Phys.* **2**, 397 (1976).
- [52] D. Pantelica, I. G. Stefan, N. Nica, M. G. Porquet, G. Duchêne, A. Astier, S. Courtin, I. Deloncle, F. Hoellinger, A. Bauchet, *et al.*, *Phys. Rev. C* **72**, 024304 (2005).
- [53] S. Raman, C. Nestor Jr, and P. Tikkanen, *Atomic Data and Nuclear Data Tables* **78**, 1 (2001).
- [54] D. J. Horen, R. L. Auble, C. Wu, D. Cline, M. Devlin, R. Ibbotson, and M. Simon, *Physical Review C* **48**, 433 (1993).
- [55] B. J. Lund, N. Bateman, S. Utku, D. Horen, and G. Satchler, *Physical Review C* **51**, 635 (1995).
- [56] M. Zielińska, L. Gaffney, K. Wrzosek-Lipska, E. Clément, T. Grahn, N. Kesteloot, P. Napiorkowski, J. Pakarinen, P. Van Duppen, and N. Warr, *Eur. Phys. J. A* **52**, 99 (2016).
- [57] N. J. Stone, *Tech. Rep. INDC(NDS)-0833 10.61092/iaea.a6te-dg7q* (2021).
- [58] T. Kibedi and R. Spear, *At. Data Nucl. Data Tables* **80**, 35 (2002).
- [59] K. Kumar, *Phys. Rev. Lett.* **28**, 249 (1972).